Magnetron Sputtered TiO_2 Films on a Stainless Steel Substrate: Selective Rutile Phase Formation and Its Tribological and Anti-corrosion Performance

Dangeti Siva Rama Krishna[a], Yong Sun[b1] and Zhong Chen[a1]

[a.] *School of Materials Science and Engineering, Nanyang Technological University, 50 Nanyang Avenue, Singapore 639798*

[b] *Department of Engineering, Faculty of Technology, De Montfort University, Leicester LE1 9BH, UK*

Abstract

In this work, TiO_2 films on 316L stainless steel have been formed by non-reactive magnetron sputtering of TiO_2 target. The effect of a titanium underlayer on the crystalline phase of the TiO_2 film has been investigated in terms of phase evolution, film morphology, corrosion resistance, adhesion strength, hardness and tribological characteristics. Results showed that the titanium underlayer has a significant effect on the phase of the TiO_2 film. Without this underlayer, an anatase TiO_2 film is produced, in consistence with many other investigations. However, it is found that with a titanium underlayer, a rutile TiO_2 film can be directly formed on the substrate. The thickness of the interface layer affects the crystallinity of the rutile film. By controlling the underlayer thickness, the resultant rutile film crystal structure and morphology could be changed accordingly. At an optimized state, the rutile coating shows much improved adhesion, friction, wear and corrosion properties.

Keywords: Titanium oxide, Tribology, Adhesion, Corrosion, Sputtering, Surface morphology

[1] Corresponding authors.
E-mail addresses: ysun01@dmu.ac.uk (Y. Sun), ASZChen@ntu.edu.sg (Z. Chen).

1. Introduction

Titanium dioxide (TiO_2) with a rutile structure is popular for its excellent combination of physical, chemical, mechanical and biomedical properties [1,2]. Increasing efforts have been made to fabricate this material in the form of thin films for various applications like chemical catalysts, optical devices and electromagnetic devices [3,4]. More recently, it has been discovered that rutile has good biocompatibility and is a potential friction-reducing and wear-resistant material, and thus has a great potential for applications in human implants, medical devices and other tribological applications [5,6]. However, very few efforts have been made so far in the fabrication and characterisation of rutile films on substrates other than titanium for potential tribological applications. In addition, obtaining a complete rutile film, even from a rutile target, on any substrate requires tedious post heat treatments to transform it from anatase and/or amorphous phases, which have poor tribological properties than rutile. And the rutile phase could only be formed after post treatment of the metastable phases [7,8].

A novel technique has been investigated in the present work to fabricate a rutile-TiO_2 based film on AISI 316L austenitic stainless steel, which is a technologically important material used widely in various sectors of industry. The technique involves the deposition of a titanium underlayer onto AISI 316L stainless steel by magnetron sputtering first, followed by the deposition of a rutile film on top. The present paper discusses the effect of underlayer on the structural, tribological and corrosion properties of the subsequent TiO_2 films.

2. Experiment

Surgical grade AISI 316L austenitic stainless steel was used as the substrate in the present study. Surface preparation was carried out by grinding followed by polishing with one-micron diamond paste. Before sputter deposition, the specimens were ultrasonically cleaned in acetone and ethanol. Initially the specimens were sputter cleaned for 20 minutes by

applying a RF discharge with a power of 150W applied to the substrate only. Titanium underlayers were deposited on the specimens by sputtering a 6-inch titanium target of 99.99% purity with a power of 300 W in a DC magnetron sputtering system (MSS3 manufactured by Coaxial, UK). TiO_2 films were deposited on top of the Ti underlayer by sputtering a rutile target for 120 minutes at a RF power of 200 W. The working pressure of Ar gas was 0.5 Pa and the substrate temperature was 300°C. No bias was applied to the substrate during the film deposition process.

The phase constituents of the films were analysed by glancing incidence angle X-ray diffraction (GIXD), at an incidence angle of 2^o using Cu-K_α radiation. Film thickness was measured by making a ball-crater [9,10] on the film surface by standard ball-crater testing using the CSEM Calotest machine. The surface morphology of the films was observed under field emission scanning electron microscopy (FESEM). The hardness of the films was measured by nanoindentation using NanoTest Tm instrument manufactured by Micro Materials Ltd. (UK), with a Berkovich diamond indenter. The modified Oliver and Pharr method [11] was used to calibrate the machine compliance and indenter tip area function and to analyse the indentation load–displacement data. The microscratch mode of the Nanotest machine was adopted to assess the adhesion strength of the coating to the substrate. The test involved drawing a diamond stylus of 25 μm radius over the coating surface at a constant travelling speed of 5 $\mu m\, s^{-1}$ and at continuously increasing load. The critical load at which adhesive failure of the coating occurred was detected by optical microscopic examination of the scratch track after the test, and was used as a measure of the coating adhesion strength.

Unlubricated sliding friction and wear tests were carried out using the ball-on-disc tribometer (CSEM Instruments) at room temperature and ambient conditions. An alumina ball of 6 mm in diameter was used as the counterface. During the test, the specimen to be tested was rotating against the stationary ball under applied normal loads of 1N and 3N. The

sliding speed of the specimen relative to the ball was 5 cm/s and the total sliding laps were 3744 (equivalent to 200 m sliding distance). The friction coefficient of the sliding couple was recorded continuously during the test by a computer data-requisition system. The wear volume from the specimen was evaluated after the test, by measuring the surface profile across the wear track using a surface profilometer. The wear volume was then normalised with the sliding distance and the applied load to obtain the wear rate.

The corrosion behaviour of the specimens was tested in an electrolyte of 3wt.% NaCl solution. An electrochemical corrosion test was carried out in a flat cell, with the specimen-exposed area of $1cm^2$. Anodic polarization curves were measured potentiodynamically at a scan rate of 0.5 mV/s starting from −250 mV (vs. E_{corr}) to 1000 mV (vs. SCE) with a potentiostat (ACM, UK) at room temperature. Before anodic polarization scanning, the specimen was kept at the open-circuit potential for 20 min to allow dynamic stabilization between the working electrode and the electrolyte.

3. Results and Discussion

3.1 Rutile TiO_2 film formation

In the present study, TiO_2 films were deposited on the stainless steel substrate with and without a Ti underlayer to understand the effect of an underlayer on the structural and other properties of the TiO_2 film. The effect of underlayer thickness was studied by sputtering the Ti target for various durations from 30 to 120 minutes. Fig.1 shows the crater made on the surface of the TiO_2 film on Ti underlayer deposited for 60 minutes by stainless steel ball of 25 mm diameter. It clearly shows a Ti underlayer well adhered to the stainless steel substrate. Sputter deposition of Ti underlayer for 30, 60 and 120 min resulted in 0.16, 0.44 and 0.92 μm thicknesses, respectively. Fig.2 shows the GIXD patterns of the TiO_2 films with and without an underlayer obtained at an incidence angle of 2^o. XRD pattern of the TiO_2 film

without underlayer (sample labeled with 0 underlayer thickness) shows peaks corresponding to anatase-TiO_2, along with peaks from the stainless steel substrate, indicating anatase as a major phase in the film. We have also carried out deposition under the same conditions using other substrates such as silicon wafer, Ti metal and Ti alloy, and even rutile TiO_2 surface prepared by thermal oxidation of Ti. Invariably, anatase phase was observed. Whereas in the as-deposited films on Ti underlayer, diffraction peaks corresponding to rutile and Ti were detected on 0.16 and 0.44 μm thick (corresponding to 30 and 60 min deposition) underlayer substrates. Amorphous TiO_2 was observed on the thickest (0.92 μm, corresponding to 90 min deposition) underlayer (Fig. 2). Therefore the apparent condition for the formation of rutile TiO_2 film under relatively low substrate temperature (300°C) is that it requires a thin layer of Ti as the underlayer before sputtering.

Why rutile phase only forms under such a condition is of interest. It is clearly related to the favorable heterogeneous nucleation condition provided by the Ti underlayer surface. Fig. 3 shows XRD profiles of Ti films with different thicknesses. Interestingly, underlayers of 0.16 and 0.44 μm thick, which promoted rutile formation in oxide layer showed only a single (100) Ti peak in the XRD profile. Whereas, in the thick underlayer (0.92 μm) that amorphous TiO_2 formed, both Ti (100) and (002) peaks were prominent, along with another two relatively weak peaks corresponding to (101) and (102) planes. The (100) texture appears to be the condition for rutile TiO_2 formation. The reason for this (100) texture formation is due to the presence of oxygen impurity, which helps in minimizing the surface energy of (100) component against the closely packed (002) in Ti. Similar observation of impurity impact on surface energy minimization and texture formation is reported elsewhere [12]. Composition measurement on the cross section TEM samples confirmed that the oxygen concentration is high (~10 at%) in the Ti layer deposited for 60 min or below, but it decreases significantly in the 120 min deposited Ti underlayer. The variation in film oxygen content is due to the

variation of oxygen residues in the sputter chamber. Ti is a well known oxygen getter; it incorporates oxygen residues even for deposition conducted in ultra high vacuum systems. During the early stage of deposition, oxygen dissolved into the film easily. However, with extended deposition time, the availability of the oxygen residues in the chamber decreases, resulting in low oxygen concentration in thick Ti underlayer.

The morphology of the TiO_2 films deposited on the stainless steel substrate with and without Ti underlayers are shown in Fig. 4. There is a great difference between the morphologies of the TiO_2 films deposited on Ti underlayers (Fig. 4b-d) and that deposited directly on the stainless steel substrate (Fig. 4a). In the case of TiO_2 films deposited directly on the stainless steel substrate, where anatase phase formed, morphology showed square-based pyramidal grains with narrow size distribution. On the oxide layers on Ti underlayer, islands with relatively large average size were observed. There is a clear distinction between the films with an amorphous (Fig. 4d) and a rutile phase (Fig. 4b & c). Films with amorphous phase show globular islands with increased roughness and average nodule size compared to rutile films. Comparing the two rutile films (Fig. 4b & c), the grain size, as inferred by the peak broadening in Fig. 2, is smaller with the 0.44 μm thick underlayer.

3.2 Mechanical and anti-corrosion performance

Fig.5 shows the hardness values determined by nanoindentation of the films to a depth of 100 nm. The TiO_2 film was about 450 nm thick, therefore the obtained hardness value may not be completely free of influence from the substrate. Nevertheless since the indentation depth is about 1/5 of the film thickness, we believe the trend in measured hardness is mainly caused by the film true hardness. It is clearly observed that the films with an underlayer show higher hardness as rutile is harder than anatase. Within the rutile films, it can be seen that hardness increases with the increase in underlayer thickness. This is because of the decrease

in the crystallite size with increasing underlayer thickness. However, the hardness drops with further increasing underlayer thickness when TiO_2 film becomes amorphous on the thickest (0.96 μm) Ti underlayer.

Fig.6 compares the scratch tracks on TiO_2 films caused by microscratch test. Close observation of the scratch tracks finds that there is difference in the width of the tracks among different samples. The tracks of the samples 0 and 0.92 are wider than the other two and especially sample 0.44 shows the narrowest track among all. This seems to correlate well with the hardness of the film. The critical load (Lc) in the scratch adhesion test is a measure of adhesive strength in the absence of complete delamination of the film with substrate [13]. Fig.7 shows the critical loads (Lc) of all the samples obtained by the microscratch test. It can be seen that the critical load to adhesive failure increases when the underlayer is present in comparison to the film without a Ti underlayer. It can be understood that a ductile and compliant metallic (Ti) underlayer can relax the residual stresses caused due to the sputter deposition of the TiO_2 films. However, a sudden decrease in critical load for the TiO_2 film on the thickest Ti underlayer can be seen from the figure. This is also attributed to the presence of amorphous TiO_2 and higher surface roughness. The rougher surface in the film acts as stress raisers which deteriorates the anti-scratch performance.

Unlubricated sliding friction and wear tests have been carried out under a load of 1N and 3N. Fig. 8 shows the friction coefficient versus distance plots recorded during the tribology test at a load of 1N. Both sample 0 and 0.16 exhibit high friction and large fluctuation, a phenomenon typical of poor tribological materials which show adhesive wear and stick-slip tendency. On the other hand, the friction curve for the samples with a thick Ti underlayer, samples 0.44 and 0.92, is smooth with much reduced friction coefficient values and less fluctuation. The mean friction coefficients of the contacts between the ball and the TiO_2 surfaces are 0.512, 0.479, 0.377 and 0.382 for samples on 0, 0.16, 0.44 and 0.92 μm Ti

underlayer, respectively. It shows that the coefficient of friction decreases with creasing underlayer thickness. The sample with no underlayer and the least thick underlayer show relatively high friction coefficients as the sliding media reach the metallic substrate. The effect of the Ti-underayer thickness on the friction can be explained by its role to provide adhesion between the rutile film and the substrate. The sample with a 0.16 μm Ti underlayer rutile film shows high fluctuation in the friction coefficient after ~1000 laps (Fig. 8), indicating that the substrate has lost the protection. Microscopic examination of the wear tracks shows that the TiO_2 film without a Ti underlayer suffered from large amount of wear, where severe adhesive wear, together with surface and subsurface plastic deformation occurred, such that a wide, deep and rough wear track was produced (Fig.9). In contrast, the wear track produced on the samples with underlayer has a very smooth and polished appearance, especially sample 0.44 shows very narrow wear track. Fig. 10 shows the wear rates calculated by measuring the volume loss from the surfaces of the tested samples. However, for the films that failed under 1 N load during pin on disc test, testing was not further done under 3 N. It was found that in the case of films on Ti underlayer, the wear rate decreased with respect to the TiO_2 film without the underlayer, contributing from the superior tribological properties of rutile over anatase. Further, the wear rate decreased with the increase in the underlayer thickness for the reason discussed above. However, similar to the case of hardness and adhesion strengths, an increased wear rate was observed for the TiO_2 film on the thickest Ti underlayer. This can also be attributed to the poor density of TiO_2 with voids and pores in the amorphous film.

The potentiodynamic polarization curves of the selected TiO_2 films substrate samples are shown in Fig. 11. By comparing the curves, two salient differences between the electrochemical behaviour of the uncoated substrate and TiO_2 film can be seen. First, the current density at any given potential for the TiO_2 film is always lower than that of the

uncoated substrate. Second, the polarization curve in the reverse sweep of the cyclic test follows the same trend for the TiO_2 films. The results show that the formation of a rutile-TiO_2 based film on 316L steel improves the general corrosion resistance of the steel in the chloride solution.

4. Conclusions

The work reported in this paper has demonstrated that the phase composition of the TiO_2 films on the stainless steel substrate is influenced by the Ti underlayer, resulting in the formation of rutile-TiO_2 without the requirement of post treatment. The thickness of Ti underlayer also has significant influence on the phase composition and properties of the resultant films. Controlled formation of rutile TiO_2 films can significantly enhance the surface hardness, tribological properties and corrosion resistance of the stainless steel in terms of much reduced friction coefficient and increased wear resistance. The TiO_2 film with an underlayer of about 0.44 μm thick, obtained by 60 min Ti underlayer sputter deposition, shows high hardness, good adhesion strength, best wear resistance, and improved corrosion resistance in the chloride solution.

References

[1] U. M.Diebold, Surf. Sci. Rep. 48 (2003) 3.

[2] D. Stamate Marius, Appl. Surf. Sci. 205 (2003) 353.

[3] P. Lobl, M. Huppertz, D. Mergel, Thin Solid Films. 251 (1994) 72.

[4] Nilson C. da Cruz, Surf. Coat. Technol. 126 (2000) 123.

[5] M.P.Casaletto, G.M.Ingo, S.Kaciulis, G.mattogno, Appl. Surf. Sci. 172 (2001)167.

[6] Y.X.Leng, P.K.Chu, Surf. Coat. Technol. 156 (2002) 295.

[7] D.-J. Won, C.-H.Wang, H.-K.Jang, D.-J.Choi, Appl. Phys. A73 (2001)595.

[8] M.D.Wiggins, M.C.Nelson and C.R.Aita J. Vac. Sci. Tech. A14 (3) (1996) 772.

[9] Y. Kusano, K.V.Acker, I. M. Hutchings, Surf. Coat. Technol. 183 (2004) 312.

[10] D. Siva Rama Krishna and Y. Sun, Surf. Coat. Technol. 198 (2005) 447.

[11] W.C. Oliver, G.M. Pharr, J. Mater. Res. 7 (1992) 1564.

[12] D. B. Knorr, S. M. Merchant, M.A. Biberger, J. Vac. Sci. Technol. B., 16 (1998) 2734

[13] S. J. Bull, Trib. Int. 30(7) (1997) 491

List of figures

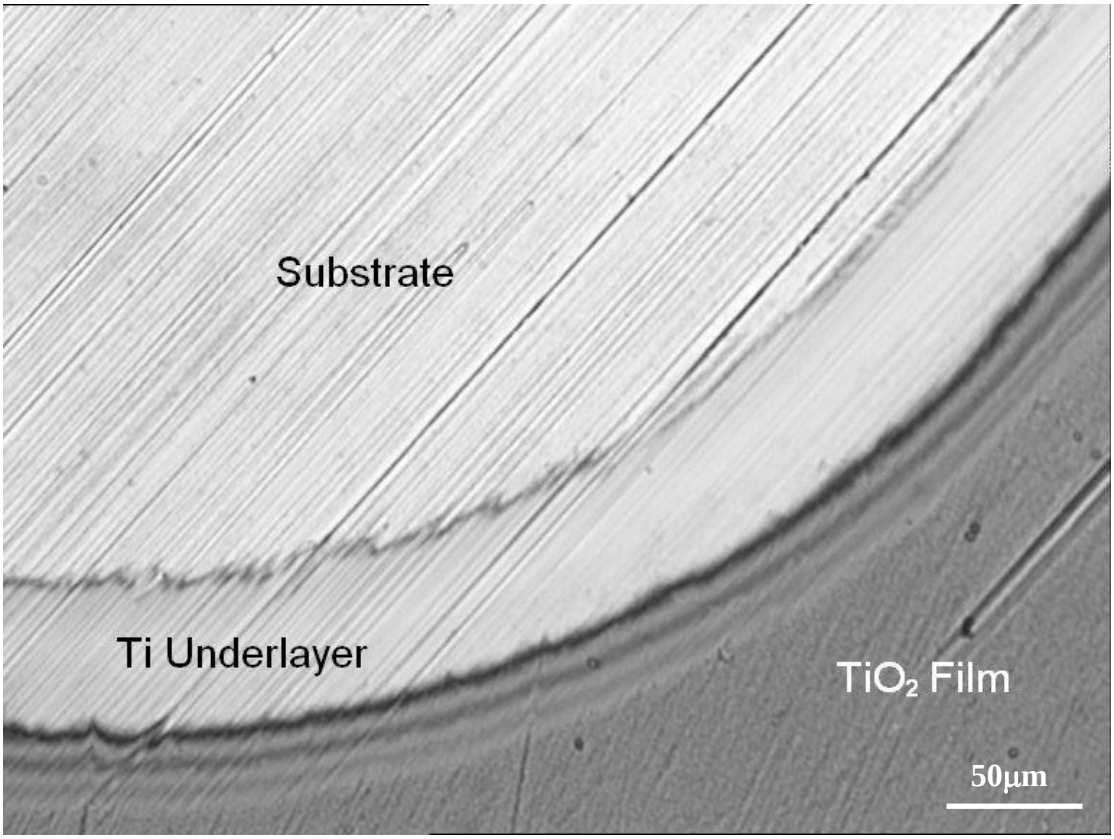

Figure 1

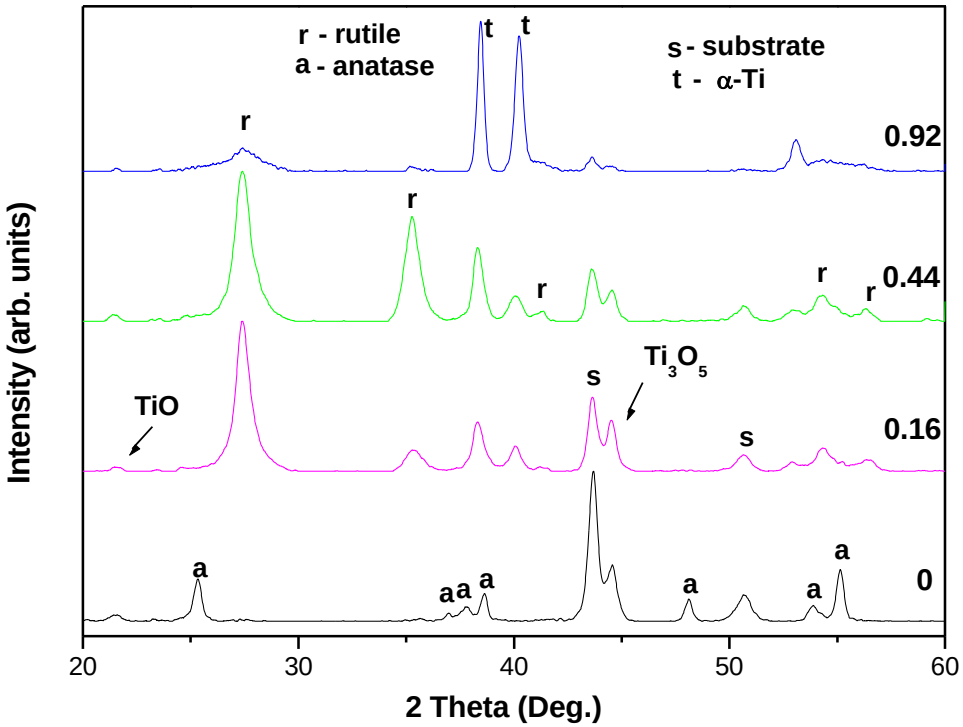
r - rutile
a - anatase
s - substrate
t - α-Ti
0.92
0.44
0.16
0
TiO
Ti3O5
Intensity (arb. units)
2 Theta (Deg.)
20
30
40
50
60

Figure 2

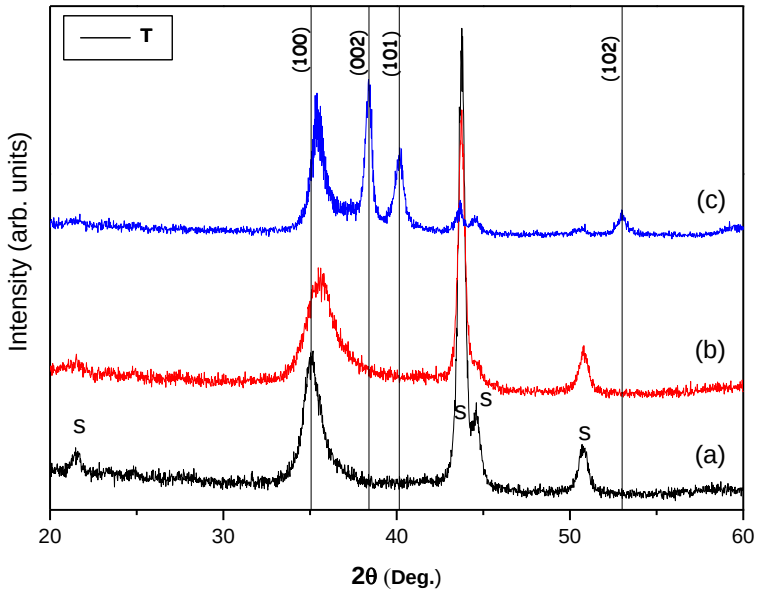
T
(100)
(002)
(101)
(102)
(c)
(b)
(a)
S
S
S
S
Intensity (arb. units)
20
30
40
50
60
2θ (Deg.)

Figure 3

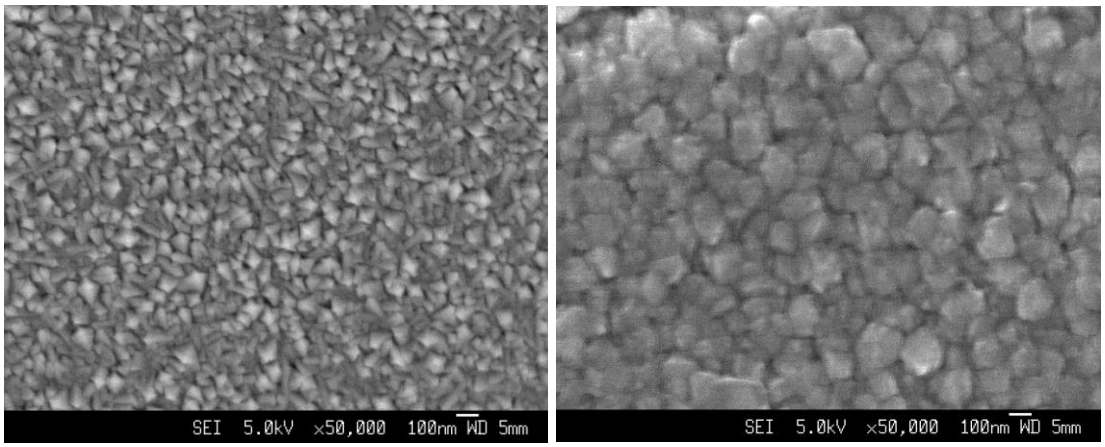

(a) (b)

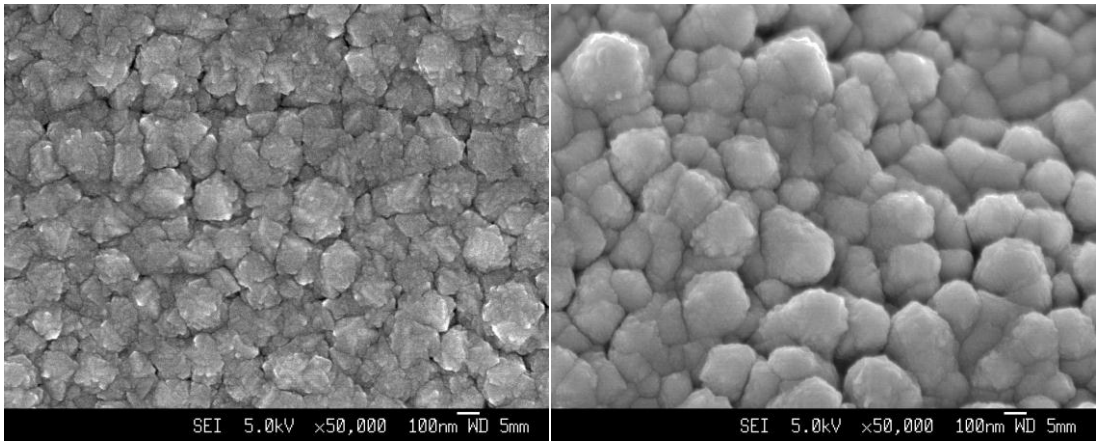

(c) (d)

Figure 4

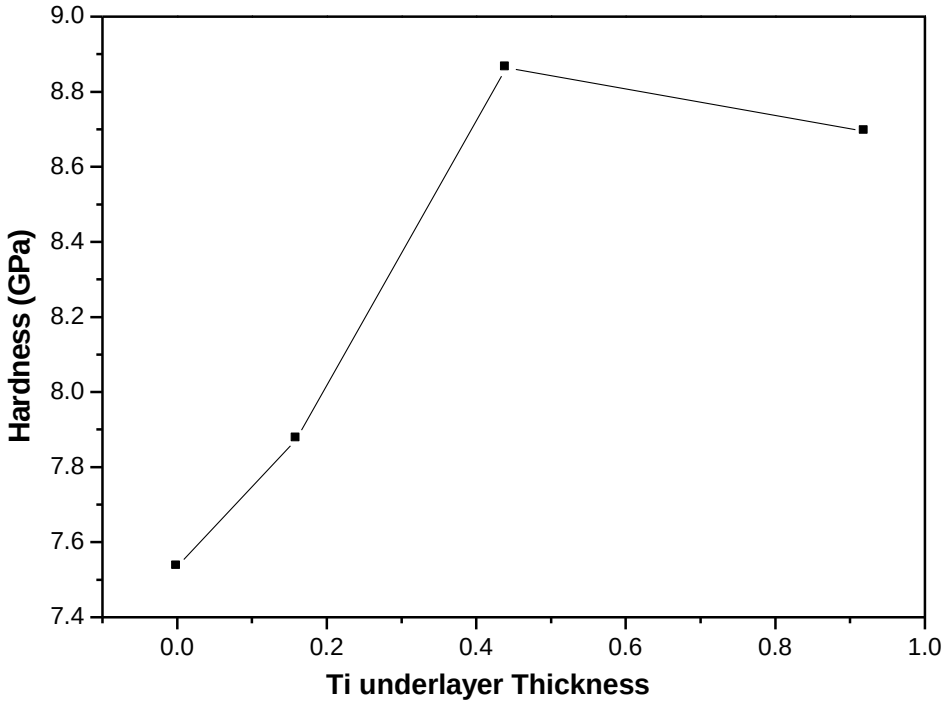
9.0
8.8
8.6
8.4
8.2
8.0
7.8
7.6
7.4
Hardness (GPa)
0.0
0.2
0.4
0.6
0.8
1.0
Ti underlayer Thickness

Figure 5

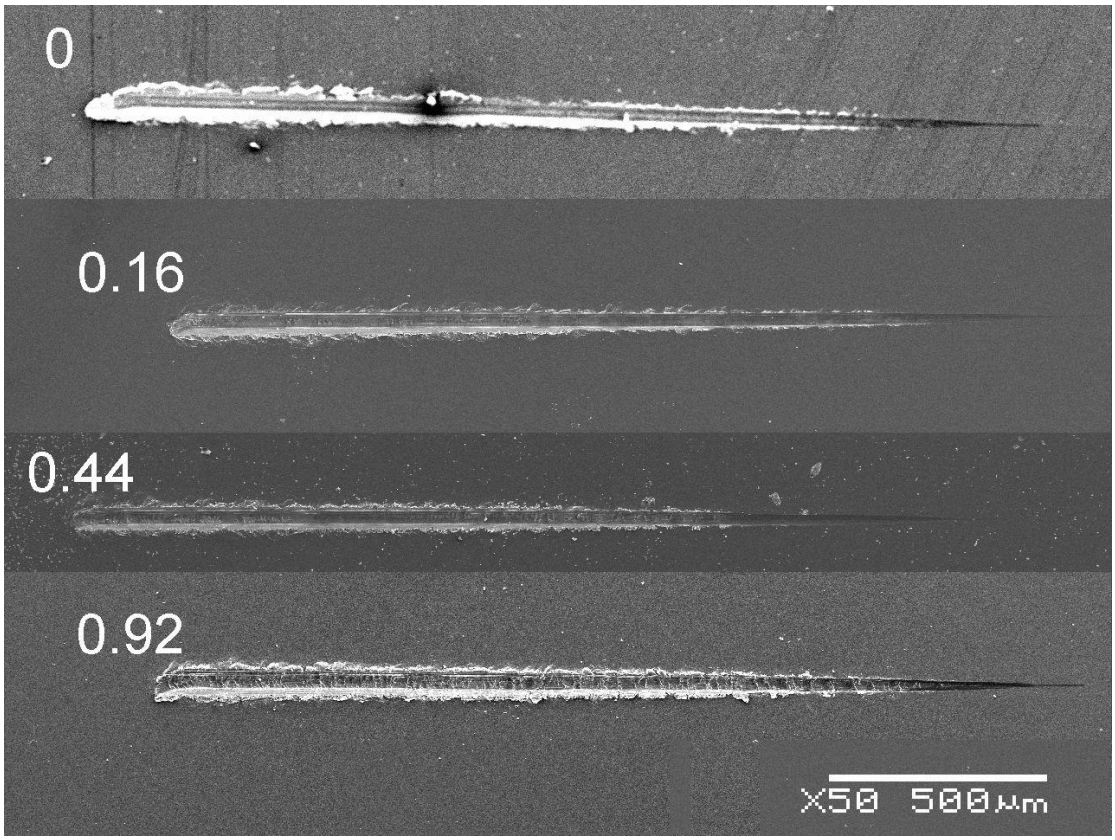

Figure 6

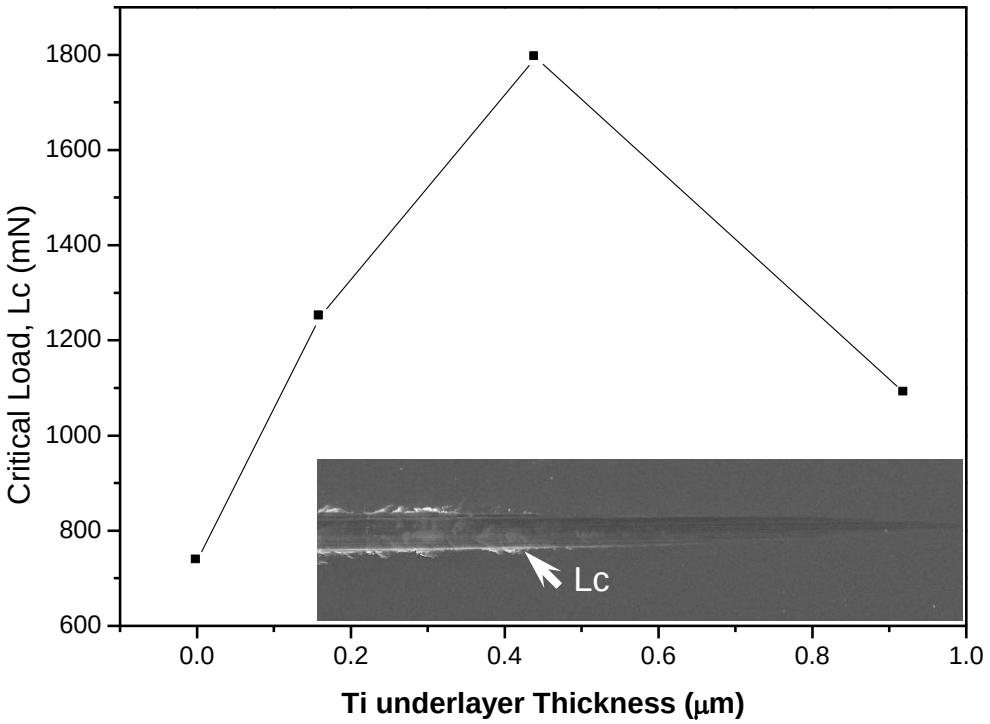
Critical Load, Lc (mN)
1800
1600
1400
1200
1000
800
600
0.0
0.2
0.4
0.6
0.8
1.0
Ti underlayer Thickness (μm)
Lc

Figure 7

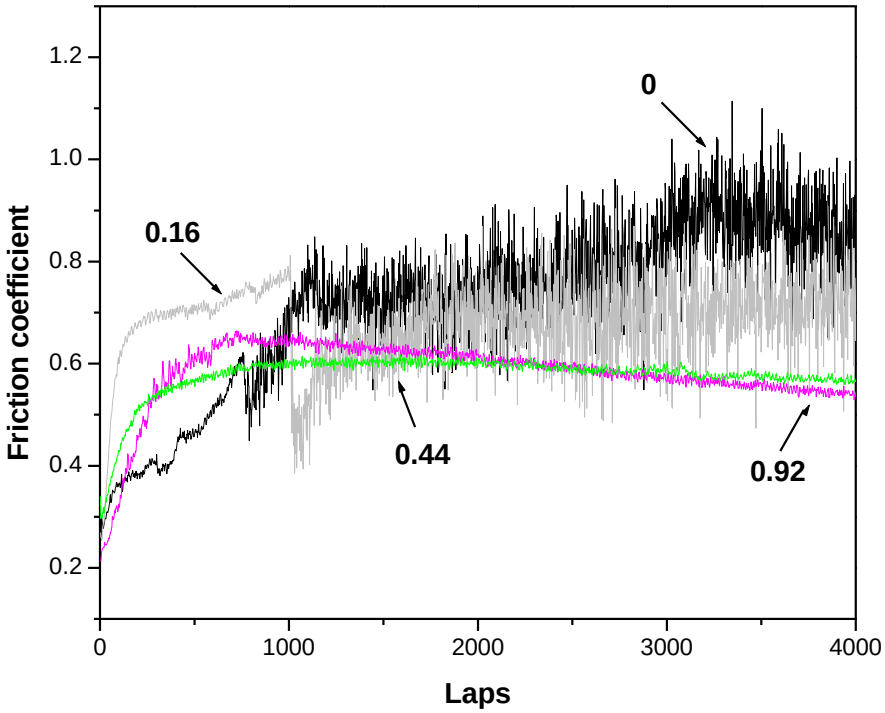
Friction coefficient
Laps
0
0.16
0.44
0.92
1.2
1.0
0.8
0.6
0.4
0.2
0
1000
2000
3000
4000

Figure 8

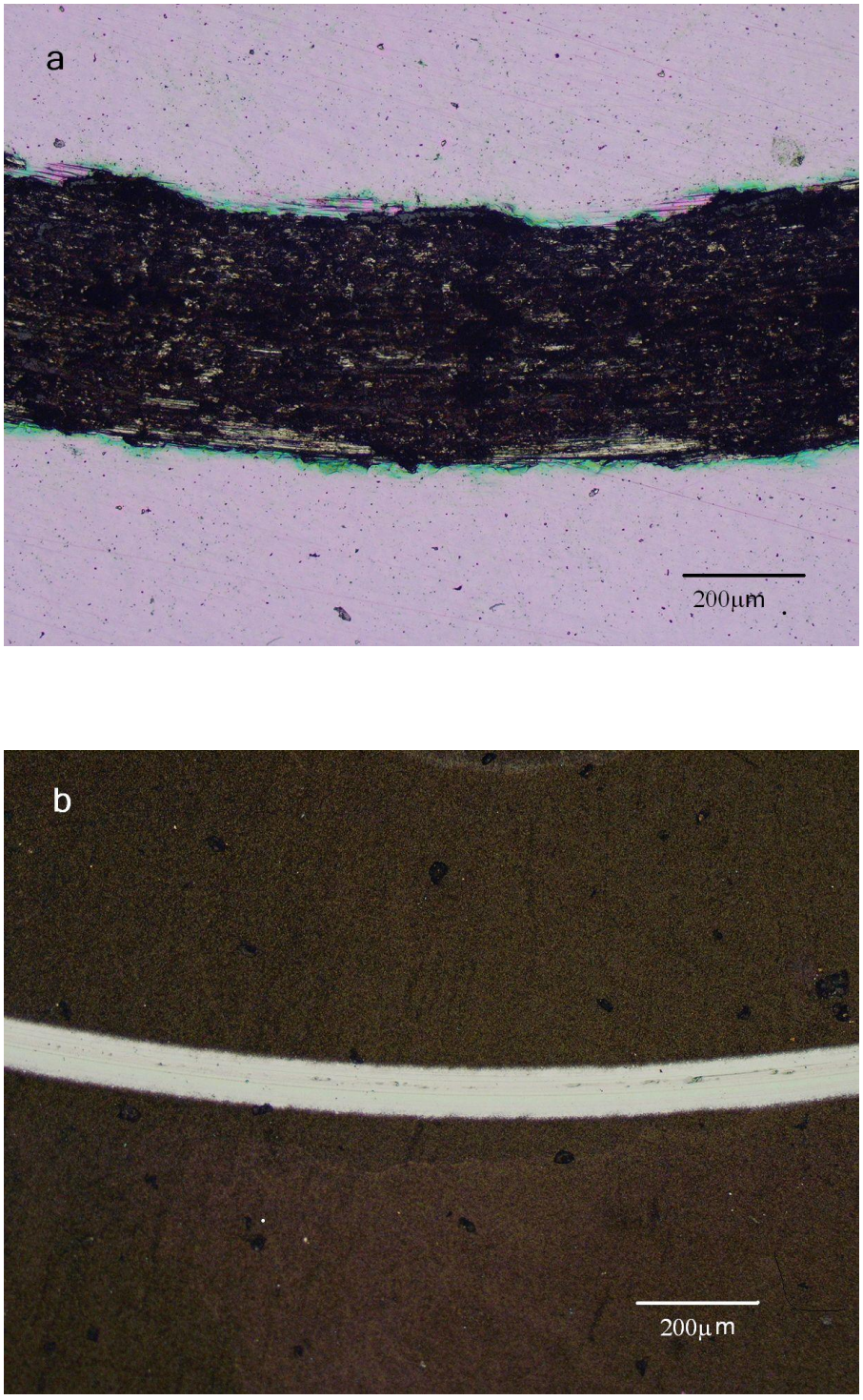

Figure 9

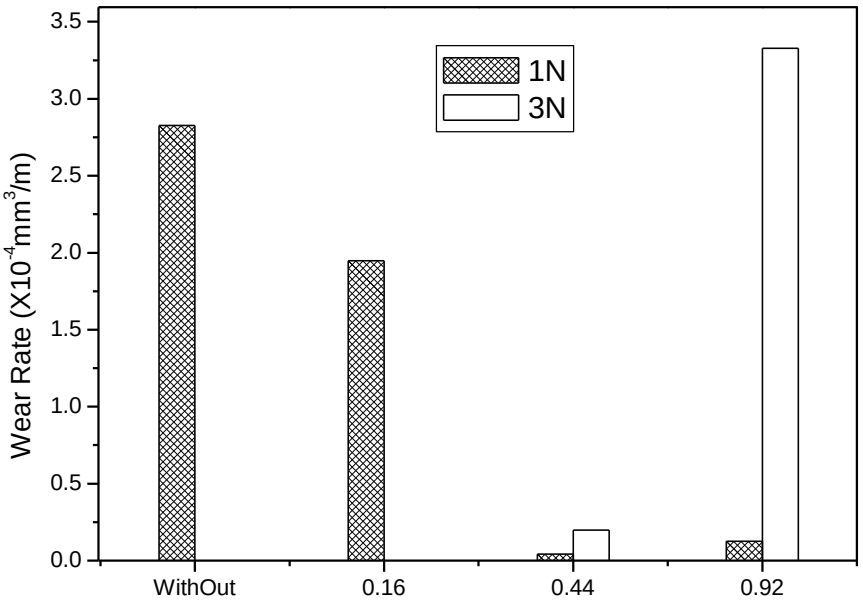
3.5
3.0
2.5
2.0
1.5
1.0
0.5
0.0
Wear Rate (X10-4mm3/m)
1N
3N
WithOut
0.16
0.44
0.92

Figure 10

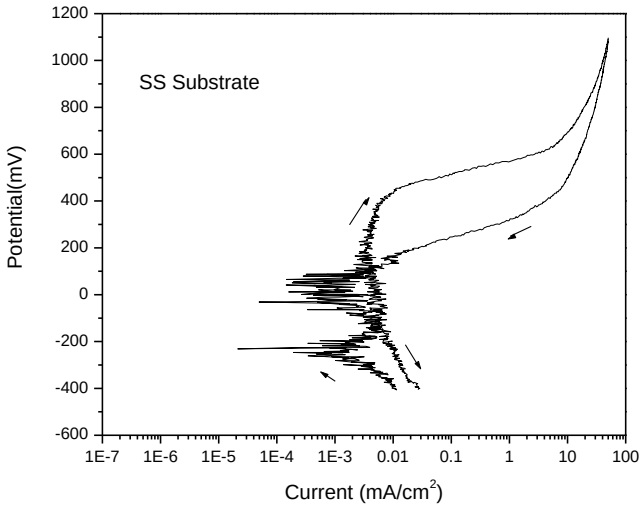
SS Substrate
Potential(mV)
1200
1000
800
600
400
200
0
-200
-400
-600
1E-7
1E-6
1E-5
1E-4
1E-3
0.01
0.1
1
10
100
Current (mA/cm2)

(a)

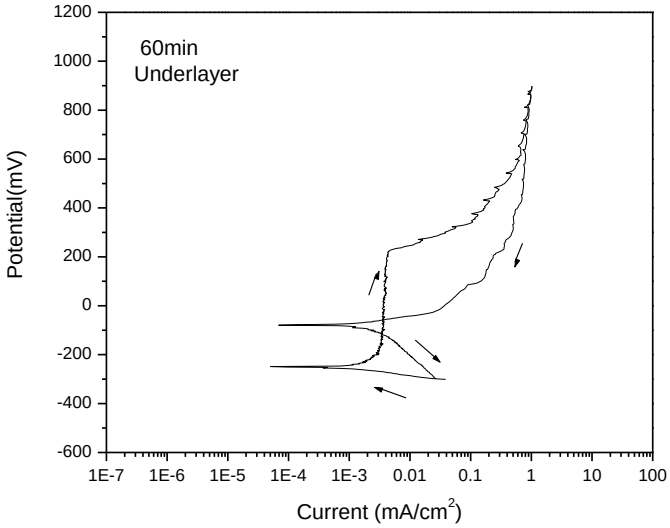
60min
Underlayer
Potential(mV)
1200
1000
800
600
400
200
0
-200
-400
-600
1E-7
1E-6
1E-5
1E-4
1E-3
0.01
0.1
1
10
100
Current (mA/cm2)

(b)

Figure 11